

# Correction of sampling errors due to laser tuning rate fluctuations in swept-wavelength interferometry

Eric D. Moore and Robert R. McLeod

Department of Electrical and Computer Engineering, University of Colorado at Boulder, 425 UCB, Boulder, CO 80309

[Eric.Moore@Colorado.edu](mailto:Eric.Moore@Colorado.edu)

**Abstract:** The frequency-sampling method is widely used to accommodate nonlinear laser tuning in swept-wavelength interferometric techniques such as optical frequency domain reflectometry (OFDR) and swept-wavelength optical coherence tomography (OCT). In this paper we analyze the frequency-sampling method and identify two sources of sampling errors. One source of error is the limit of an underlying approximation for long interferometer path mismatches and fast laser tuning rates. A second source of error is transmission delays in data acquisition hardware. We show that the measurement system can be configured such that the two error sources cancel to second order. We present experimental verification of sampling error correction using a general swept-wavelength interferometer with a significantly nonlinear laser sweep.

© 2008 Optical Society of America

**OCIS codes:** (060.2300) Fiber measurements; (120.3180) Interferometry.

---

## References and links

1. A. Hymans and J. Lait, "Analysis of a frequency-modulated continuous-wave ranging system," *Proc. IEEE* **107**, 365–372 (1960).
2. E. C. Burrows and K.-Y. Liou, "High resolution laser LIDAR utilising two-section distributed feedback semiconductor laser as a coherent source," *Electron. Lett.* **26**, 577–579 (1990).
3. W. Eickhoff and R. Ulrich, "Optical frequency domain reflectometry in single-mode fiber," *Appl. Phys. Lett.* **39**, 693–695 (1981).
4. S. A. Kingsley and D. E. N. Davies, "OFDR diagnostics for fibre and integrated-optic systems," *Electron. Lett.* **21**, 434–435 (1985).
5. D. Uttam and B. Culshaw, "Precision time domain reflectometry in optical fiber systems using a frequency modulated continuous wave ranging technique," *J. Lightwave Technol.* **LT-3**, 971–977 (1985).
6. U. Glombitza and E. Brinkmeyer, "Coherent frequency-domain reflectometry for characterization of single-mode integrated-optical waveguides," *J. Lightwave Technol.* **11**, 1377–1384 (1993).
7. J. P. von der Weid, R. Passy, G. Mussi, and N. Gisin, "On the characterization of optical fiber network components with optical frequency domain reflectometry," *J. Lightwave Technol.* **15**, 1131–1141 (1997).
8. L.-T. Wang, K. Iiyama, F. Tsukada, N. Yoshida, and K.-I. Hayashi, "Loss measurement in optical waveguide devices by coherent frequency-modulated continuous-wave reflectometry," *Opt. Lett.* **18**, 1095–1097 (1993).
9. R. Passy, N. Gisin, and J. P. von der Weid, "High-sensitivity-coherent optical frequency-domain reflectometry for characterization of fiber-optic network components," *IEEE Photon. Technol. Lett.* **7**, 667–669 (1995).
10. M. Froggatt, T. Erdogan, J. Moore, and S. Shenk, "Optical frequency domain characterization (OFDC) of dispersion in optical fiber Bragg gratings," in *Bragg Gratings, Photosensitivity, and Poling in Glass Waveguides*, OSA Technical Digest Series, pp. 176–178 (Optical Society of America, 1999).
11. M. Yoshida, K. Nakamura, and H. Ito, "A new method for measurement of group velocity dispersion of optical fibers by using a frequency-shifted feedback fiber laser," *IEEE Photon. Technol. Lett.* **13**, 227–229 (2001).
12. T.-J. Ahn, Y. Jung, K. Oh, and D. Y. Kim, "Optical frequency-domain chromatic dispersion measurement method for higher-order modes in an optical fiber," *Opt. Express* **13**, 10,040–10,047 (2005).

13. M. Froggatt, "Distributed measurement of the complex modulation of a photoinduced Bragg grating in an optical fiber," *Appl. Opt.* **35**, 5162–5164 (1996).
14. H. Rosenfeldt, C. Knothe, J. Cierullies, and E. Brinkmeyer, "Evolution of amplitude and dispersion spectra during fiber Bragg grating fabrication," in *Bragg Gratings, Photosensitivity, and Poling in Glass Waveguides*, OSA Technical Digest Series (Optical Society of America, 2001).
15. O. H. Waagaard, "Spatial characterization of strong fiber Bragg gratings using thermal chirp and optical-frequency-domain reflectometry," *J. Lightwave Technol.* **23**, 909–914 (2005).
16. B. Huttner, J. Reece, N. Gisin, R. Passy, and J. P. von der Weid, "Local birefringence measurements in single-mode fibers with coherent optical frequency-domain reflectometry," *IEEE Photon. Technol. Lett.* **10**, 1458–1460 (1998).
17. M. Yoshida, T. Miyamoto, N. Zou, K. Nakamura, and H. Ito, "Novel PMD measurement method based on OFDR using a frequency-shifted feedback fiber laser," *Opt. Express* **9**, 207–211 (2001).
18. M. Wegmuller, M. Legré, and N. Gisin, "Distributed beatlength measurement in single-mode fibers with optical frequency-domain reflectometry," *J. Lightwave Technol.* **20**, 800–807 (2002).
19. M. Froggatt and J. Moore, "High-spatial-resolution distributed strain measurement in optical fiber with Rayleigh backscatter," *Appl. Opt.* **37**, 1735–1740 (1998).
20. M. Froggatt, B. Soller, D. Gifford, and M. Wolfe, "Correlation and keying of Rayleigh scatter for loss and temperature sensing in parallel optical networks," in *Optical Fiber Communication Conference*, OSA Technical Digest Series (Optical Society of America, 2004). Paper PDP17.
21. D. K. Gifford, B. J. Soller, M. S. Wolfe, and M. E. Froggatt, "Distributed fiber-optic temperature sensing using Rayleigh backscatter," in *European Conference on Optical Communication*, vol. 3 of *ECOC 2005 Proceedings* (2005). Paper We4.P.005.
22. B. J. Soller, D. K. Gifford, M. S. Wolfe, M. E. Froggatt, M. H. Yu, and P. F. Wysocki, "Measurement of localized heating in fiber optic components with millimeter spatial resolution," in *Optical Fiber Communication Conference and Exposition and the National Fiber Optic Engineers Conference*, Technical Digest (CD) (Optical Society of America, 2006). Paper OFN3.
23. M. Froggatt, D. Gifford, S. Kreger, M. Wolfe, and B. Soller, "Distributed strain and temperature discrimination in unaltered polarization maintaining fiber," in *Optical Fiber Sensors*, OSA Technical Digest (CD) (Optical Society of America, 2006). Paper ThC5.
24. G. D. VanWiggeren, A. R. Motamedi, and D. M. Baney, "Single-scan interferometric component analyzer," *IEEE Photon. Technol. Lett.* **15**, 263–265 (2003).
25. B. J. Soller, D. K. Gifford, M. S. Wolfe, and M. E. Froggatt, "High resolution optical frequency domain reflectometry for characterization of components and assemblies," *Opt. Express* **13**, 666–674 (2005).
26. D. K. Gifford, B. J. Soller, M. S. Wolfe, and M. E. Froggatt, "Optical vector network analyzer for single-scan measurements of loss, group delay, and polarization mode dispersion," *Appl. Opt.* **44**, 7282–7286 (2005).
27. S. R. Chinn, E. A. Swanson, and J. G. Fujimoto, "Optical coherence tomography using a frequency-tunable optical source," *Opt. Lett.* **22**, 340–342 (1997).
28. S. H. Yun, G. J. Tearney, J. F. de Boer, N. Itimbia, and B. E. Bouma, "High-speed optical frequency-domain imaging," *Opt. Express* **11**, 2953–2963 (2003).
29. K. Tsuji, K. Shimizu, T. Horiguchi, and Y. Koyamada, "Spatial-resolution improvement in long-range coherent optical frequency domain reflectometry by frequency-sweep linearisation," *Electron. Lett.* **33**, 408–410 (1997).
30. K. Iiyama, L.-T. Wang, and K. ichi Hayashi, "Linearizing optical frequency-sweep of a laser diode for FMCW reflectometry," *J. Lightwave Technol.* **14**, 173–178 (1996).
31. K.-Y. Huang and G. M. Carter, "Coherent optical frequency domain reflectometry (OFDR) using a fiber grating external cavity laser," *IEEE Photon. Technol. Lett.* **6**, 1466–1468 (1994).
32. M. Kobayashi, K. Takada, and J. Noda, "Optical-frequency encoder using polarization-maintaining fiber," *J. Lightwave Technol.* **8**, 1697–1702 (1990).
33. K. Takada, "High-resolution OFDR with incorporated fiber-optic frequency encoder," **4**, 1069–1072 (1992).
34. T.-J. Ahn and D. Y. Kim, "Analysis of nonlinear frequency sweep in high-speed tunable laser sources using a self-homodyne measurement and Hilbert transformation," *Appl. Opt.* **46**, 2394–2400 (2007).

---

## 1. Introduction

Swept-wavelength interferometry (SWI) is a versatile measurement technique that has found a wide range of applications. An early use of SWI was to perform free-space ranging measurements using the technique known as frequency-modulated continuous-wave radar [1]. Similar ranging measurements have also been performed using SWI at optical wavelengths [2]. The most common use of SWI at optical wavelengths has been for measurements of reflections and backscatter in optical fibers [3, 4, 5, 6, 7]. In this context, SWI is typically referred to as optical frequency domain reflectometry (OFDR). Variations of OFDR have been used for a wide vari-

ety of measurements in fiber and integrated-optic systems, including loss [3, 8, 9], group delay and group velocity dispersion [10, 11, 12], grating characterization [13, 14, 15], birefringence and polarization mode dispersion [16, 17, 18], and distributed temperature and strain sensing [19, 20, 21, 22, 23]. In some cases a single SWI system performs several such measurements simultaneously [24, 25, 26]. SWI has also been applied to high-resolution three-dimensional imaging by combining OFDR with a raster-scanning system in a technique known as swept-wavelength optical coherence tomography (OCT) [27, 28].

All these technologies use the same core SWI system, namely a tunable laser source capable of a continuous wavelength sweep and an interferometer comprising a fixed reference path and a measurement path. All SWI systems also rely on the ability to apply a Fourier transform to the measured interference fringes. In practical systems this Fourier transform is generally applied using the fast Fourier transform (FFT) algorithm, which imposes the requirement that data be sampled at equal intervals of the independent variable. (Use of a discrete Fourier transform avoids this requirement but introduces the additional necessity that the size of each unequal interval be known.) Because the independent variable of interest in these measurements is not time, but rather the instantaneous optical frequency of the laser source, any nonlinearity in the laser tuning renders simple time-synchronous sampling of the fringe data inadequate.

Historically, the problem of nonlinear laser tuning has been dealt with in three ways. One is to focus on the design and execution of a tunable laser source with a tuning curve that is linear in time [29, 30, 8, 31]. Depending on the laser source, this approach can be difficult or impossible and, in general, is less convenient than the other options. Rather than linearizing the laser sweep, a second technique uses an auxiliary interferometer to measure the laser tuning rate as it changes throughout a wavelength sweep. This information is then used to resample the fringe data from a grid of equal time intervals to a grid of equal frequency intervals [14, 15]. The third technique, the frequency-sampling method, also uses an auxiliary interferometer, but avoids the potentially large number of interpolations required for the previous technique by using the interferometer output as a clock signal to trigger data acquisition [32, 33, 6]. This method has been widely adopted because of its convenience and accuracy; however, sampling errors that result in nonuniform frequency intervals can still occur when using an interferometric clock.

In this paper we examine the limitations of the frequency-sampling method in the context of SWI systems using commercially available tunable lasers. In general these lasers exhibit significantly nonlinear tuning that can lead to sampling errors when using an interferometric clock. Specifically, two sources of sampling error will be described. The first is intrinsic in the frequency-sampling method because the frequency spacing of the output fringes is uniform only to first order [6]. The approximation of uniform frequency spacing breaks down as both interferometer path length mismatches and average laser tuning rates increase. The second source of sampling error exists in practical SWI systems employing nonideal data acquisition (DAQ) hardware in which finite optical and electronic propagation delays cause the sampled data to lag behind the clock signal by a small time interval. These delays coupled with a nonlinear laser sweep leads to a sampling grid with unequal frequency increments [14].

In the following section we derive analytic expressions for both sources of sampling error present in SWI systems that use the frequency-sampling method. Furthermore, we show that the optical system can be configured such that the two error sources cancel one another to second order. This error correction results in greater applicability of the frequency-sampling method for long interferometers and fast laser tuning. In principle, this error correction technique can be applied to any SWI system, including all of the applications of SWI outlined above. We therefore employed a general swept-wavelength interferometer implemented in optical fiber to experimentally verify sampling error correction. Section 3 describes the measurement of the laser tuning rate variations, and Sec. 4 presents the experimental arrangement and results. Our

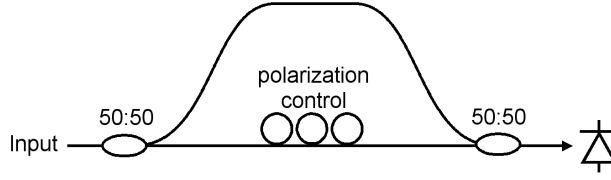


Fig. 1. An interferometer layout suitable for producing an analog clock signal for triggering swept-wavelength data acquisition.

conclusions are summarized in Sec. 5.

## 2. Sampling errors in triggered swept-wavelength interferometry

### 2.1. Sampling errors intrinsic to interferometric triggering

The schematic diagram in Fig. 1 shows the layout of an interferometer suitable for interferometric triggering implemented in single-mode optical fiber. The diagram shows a Mach-Zehnder configuration, though a Michelson or Fabry-Perot interferometer is equally applicable. In general, polarization control is required in one arm of the interferometer to avoid polarization fading of the interference fringes. To account for arbitrary nonlinear tuning of the laser source, we define the electric field at the interferometer input as

$$E(t) = E_0 e^{i\phi(t)}, \quad (1)$$

where  $\phi(t)$  is a time-varying phase and  $E_0$  is a constant amplitude. In this case the instantaneous optical frequency of the laser is given by

$$\nu(t) = \frac{1}{2\pi} \frac{d\phi}{dt}. \quad (2)$$

The input light is split by a 3 dB coupler, and the two parts are recombined after traveling different distances. We take the splitting ratio to be equal to unity for convenience; we are primarily interested in the phase of the resulting fringe pattern, and other splitting ratios will only affect the amplitude of the resulting clock signal. Also for convenience we define zero delay as the group delay through the shorter of the two paths. The group delay mismatch between the two paths is  $\tau$ . With these definitions in place, the optical fringe pattern output by the interferometer produces a voltage at the photodetector given by

$$\begin{aligned} U(t) &= \sigma |E(t) + E(t + \tau)|^2 \\ &= U_0 \{1 + \cos[\phi(t + \tau) - \phi(t)]\}, \end{aligned} \quad (3)$$

where  $\sigma$  is a constant of proportionality that depends on the detector sensitivity, and  $U_0 = 2\sigma |E_0|^2$ . Next we Taylor expand the function  $\phi(t + \tau)$  about  $t$ :

$$\phi(t + \tau) = \sum_{n=0}^{\infty} \frac{\tau^n}{n!} \phi^{(n)}(t). \quad (4)$$

Writing the zero- and first-order terms of the sum explicitly and using Eq. (2) yields an expression for the phase of the output fringe pattern:

$$\phi(t + \tau) - \phi(t) = 2\pi\nu(t)\tau + 2\pi \sum_{n=2}^{\infty} \frac{\tau^n}{n!} \nu^{(n-1)}(t). \quad (5)$$

If we neglect the second- and higher-order terms of the sum in Eq. (5), then substitution back into Eq. (3) yields a fringe pattern that is periodic in optical frequency [6]. This approximation is valid when

$$\tau^2 \frac{dv}{dt} \ll 1, \quad (6)$$

i.e., for short interferometer path length differences and/or slow laser tuning rates. In this case the frequency spacing between triggers takes on the uniform value of  $\Delta v = \tau^{-1}$ .

The preceding approximation is valid for many practical systems and has led to widespread use of the frequency-sampling method. Modern tunable lasers, however, routinely have sufficiently long coherence lengths and high tuning rates such that higher-order terms in Eq. (5) are no longer negligible. When these higher-order terms are retained, the fringe pattern output by the interferometer is no longer periodic in optical frequency. These deviations from periodicity result in nonuniform frequency intervals between trigger events; instead of the uniform interval  $\Delta v = \tau^{-1}$ , the  $i^{\text{th}}$  interval will depart from  $\tau^{-1}$  by some amount  $\delta v_i^I$ , i.e.,  $\Delta v_i = \tau^{-1} + \delta v_i^I$ . We use the superscript  $I$  to denote that the sampling error derived here is the intrinsic error present in the frequency-sampling method, distinct from sampling errors due to delays in the DAQ hardware, which are treated in the next section.

To derive an expression for the sampling error  $\delta v_i^I$ , we consider the set of times  $t_i$  at which triggers occur. These times are each separated by one period of the fringe pattern described by Eq. (3). The phase of the fringe pattern, represented in Eq. (5), will experience a change of  $2\pi$  between  $t_i$  and  $t_{i+1}$ . To express the evolution of a single period mathematically, we subtract the right side of Eq. (5) at time  $t_i$  from the same expression at time  $t_{i+1}$ , yielding

$$2\pi\tau[v(t_{i+1}) - v(t_i)] + 2\pi \sum_{n=2}^{\infty} \frac{\tau^n}{n!} [v^{(n-1)}(t_{i+1}) - v^{(n-1)}(t_i)] = 2\pi. \quad (7)$$

Rearranging terms, the change in optical frequency from one trigger event to the next can be expressed as

$$\Delta v_i \equiv v(t_{i+1}) - v(t_i) = \tau^{-1} + \delta v_i^I, \quad (8)$$

where

$$\delta v_i^I = - \sum_{n=2}^{\infty} \frac{\tau^{n-1}}{n!} [v^{(n-1)}(t_{i+1}) - v^{(n-1)}(t_i)]. \quad (9)$$

Here  $\delta v_i^I$  represents a sampling error intrinsic to interferometric triggering that depends on the interferometer path mismatch and the derivatives of the tuning rate. This error couples to the final measurement through the Fourier transform, leading to both amplitude and phase errors. These errors impose a limit on the interferometer path length differences allowable in an SWI system for a given laser that exhibits nonlinear wavelength tuning. This limit can be extended, however, by using sampling errors due to delays in the DAQ hardware to cancel the intrinsic sampling errors to second order.

## 2.2. Sampling errors due to data acquisition delays

Even when approximation (6) is valid, uniform frequency intervals between interferometrically triggered data points are still not ensured because of a second source of sampling errors: propagation delays in the DAQ hardware. Like the intrinsic sampling errors, sampling errors due to DAQ delay occur only when the wavelength sweep of the laser source is not linear in time.

To derive an expression for the sampling errors due to the DAQ delay, we begin with a detected optical trigger signal  $\tilde{U}$  that varies as a simple cosine in frequency (as is the case when higher-order sampling errors can be neglected):

$$\tilde{U}(t) = \tilde{U}_0 \{1 + \cos[2\pi v(t)\tau]\}. \quad (10)$$

Because this signal is periodic in frequency, it produces a set of trigger times  $t_i$  that correspond to sampling intervals of equal optical frequency:

$$v(t_{i+1}) - v(t_i) = \tau^{-1}. \quad (11)$$

We now introduce a fixed delay  $\delta t$  that includes two components: the differential optical delay between the trigger signal and the sampled signal, and the electronic delay between a trigger event and the moment a voltage value is recorded by the data acquisition hardware. Such a finite delay will necessarily exist because of optical and electronic transmission delays if the analog clock and data channels are not carefully path-matched. Because of this delay, the data is not sampled at the times  $t_i$ , but rather at the set of times  $t_i + \delta t$ . The effect of this delay is to perturb each frequency interval of the sampled data by an amount  $\delta v_i^D$ :

$$v(t_{i+1} + \delta t) - v(t_i + \delta t) = \tau^{-1} + \delta v_i^D. \quad (12)$$

If the laser tuning rate is constant, the change in frequency over each  $\delta t$  will be the same and  $\delta v_i^D = 0$  for all  $i$ . But if the tuning rate of the laser is changing, the frequency change over each  $\delta t$  will be different, and the frequency spacing between sampling points will no longer be uniform. To account for changes in tuning rate, we expand  $v(t + \delta t)$  as

$$v(t + \delta t) = \sum_{n=0}^{\infty} \frac{\delta t^n}{n!} v^{(n)}(t). \quad (13)$$

Substituting Eq. (13) into Eq. (12) and explicitly writing the first term of the sums yields

$$v(t_{i+1}) - v(t_i) + \sum_{n=1}^{\infty} \frac{\delta t^n}{n!} v^{(n)}(t_{i+1}) - \sum_{n=1}^{\infty} \frac{\delta t^n}{n!} v^{(n)}(t_i) = \tau^{-1} + \delta v_i^D. \quad (14)$$

Subtracting Eq. (11) from Eq. (14) results in an expression for the sampling error due to the data acquisition delay:

$$\delta v_i^D = \sum_{n=1}^{\infty} \frac{\delta t^n}{n!} [v^{(n)}(t_{i+1}) - v^{(n)}(t_i)]. \quad (15)$$

Generally speaking, the data acquisition delay  $\delta t$  can be controlled by adding a delay line to either the trigger channel or the measurement channel. Therefore it is possible to force  $\delta v_i^D = 0$  by appropriately path-matching the system such that  $\delta t = 0$ . This strategy does not always yield the best system performance, however. Instead, a nonzero sampling error due to the DAQ delay can be used to cancel the intrinsic sampling errors derived in Sec. 2.1 through a prudent choice of  $\delta t$ .

### 2.3. Correcting sampling errors

So far we have derived expressions for sampling errors due to two sources: (1) errors intrinsic to interferometric triggering due to laser tuning rate fluctuations (Eq. 9) and (2) errors that are due to delays in data acquisition hardware in the presence of laser tuning rate fluctuations (Eq. 15). When both of these errors are present, data is acquired at the times  $t_i + \delta t$ , and the frequency spacing between acquisitions is

$$\begin{aligned} \Delta v_i &= \tau^{-1} + \delta v_i^I + \delta v_i^D \\ &= \tau^{-1} - \sum_{n=1}^{\infty} \frac{\tau^n}{(n+1)!} [v^{(n)}(t_{i+1}) - v^{(n)}(t_i)] \\ &\quad + \sum_{n=1}^{\infty} \frac{\delta t^n}{n!} [v^{(n)}(t_{i+1}) - v^{(n)}(t_i)], \end{aligned} \quad (16)$$

where the summation index for  $\delta v_i^l$  has been converted from  $n$  to  $n - 1$  in order to start the summation at  $n = 1$ . It is often the case that the sampling errors are dominated by the first-order terms of the two sums. In this case we can neglect the higher-order terms, and the frequency spacing becomes

$$\Delta v_i = \tau^{-1} + [\delta t - \tau/2][v'(t_{i+1}) - v'(t_i)]. \quad (17)$$

As mentioned in the preceding section,  $\delta t$  may be controlled using delay lines in the system. Therefore, we can set  $\delta t = \tau/2$ , which will drive the error term to zero and result in a cancellation of the sampling errors. This yields error-free sampling to second order in  $\phi(t)$  and is valid as long as  $\tau^3(d^2v/dt^2) \ll 1$ .

We have shown the cancellation of the first-order error term, but it is also possible to cancel any individual term in the sum representing the total sampling error. Cancellation of an arbitrary order is possible because each successive term in the sums that constitute  $\delta v_i^l$  and  $\delta v_i^D$  differs by a factor of  $1/n$ . Therefore cancellation of any single term in the error expansion is possible through the proper choice of  $\delta t$ , but the required  $\delta t$  is different for each term. In general, to drive the  $n^{\text{th}}$  order term of the sampling error to zero, the DAQ delay must be  $\delta t = \tau(n+1)^{-1/n}$ .

### 3. Measurement of laser tuning rate variations

The preceding analysis shows that sampling errors occur when the tuning rate of the laser is not constant. To verify that the tunable laser used in the following experiment exhibits such nonlinear tuning, we measured the laser tuning rate as a function of time. This measurement was accomplished using a fiber Mach Zehnder interferometer like the one shown schematically in Fig. 1. The instantaneous tuning rate is directly related to the phase variation of the interferogram as a function of time over the course of a wavelength sweep. Ahn and co-workers described one way to perform this phase measurement using a Hilbert transform [34]. We use an alternative method based on digital filtering in the Fourier domain.

To outline the steps of the Fourier domain filtering method for characterizing nonlinear laser frequency sweeps, we will refer to experimental data shown in Fig. 2 for an Agilent 81680A tunable laser. To produce this data, the laser wavelength was swept at a nominal tuning rate of 40 nm/s. The group delay mismatch between the two arms of the interferometer was  $\tau = 13.2$  ns. The interferogram was detected using an amplified InGaAs PIN photodetector (Thorlabs PDA10CS) and sampled at 1.0 MS/s using a National Instruments PCI-6115 data acquisition card.

Figure 2(A) is a plot of the interference fringes measured during a frequency sweep. Because the differential group delay between the two paths of the interferometer is chosen such that inequality (6) is satisfied, this fringe pattern is well-described by Eq. (10). The goal of the following data processing steps is to isolate the quantity  $v(t)$  from the phase of this expression. The first step is to perform an FFT, which results in positive and negative sidebands corresponding to  $\exp[\pm i2\pi v(t)\tau]$  as shown in Fig. 2(B). Next, a digital filter is used to select a single sideband through a multiplication by the rect function overlaid on Fig. 2(B). Before transforming back to the time domain via an inverse FFT, the filtered data is shifted such that the selected sideband occupies the DC location in the data array, as shown in Fig. 2(C). The result of the inverse FFT is a data set corresponding to a single complex exponential. The phase of this exponential is plotted in red in Fig. 2(D), and the unwrapped phase is shown in black. Had we not performed the shift in the frequency domain, the phase would vary too rapidly to reliably unwrap. After unwrapping, a linear phase must be added to compensate for the shift according to the Fourier shift theorem. This results in a measurement of  $v(t)$ . A numerical derivative may then be performed to get the tuning rate.

The instantaneous tuning rate in wavelength units for the Agilent 81680A laser is shown in Fig. 2(E). The measured data show that the tuning rate oscillates about a mean value of 40 nm/s,

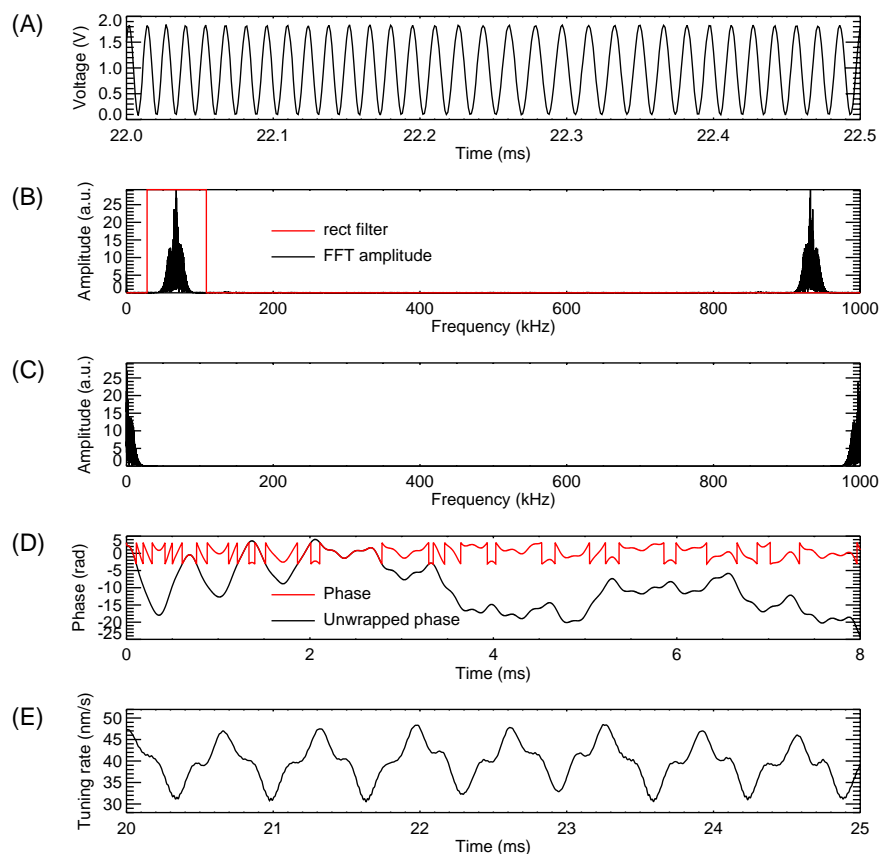


Fig. 2. (Color online) Measured data and processing steps for characterizing nonlinear laser frequency sweeps using the Fourier domain filter method. Note that different sections of the 65 ms measurement are shown in the time domain plots. (A) Measured interference fringes for an Agilent 81680A laser swept at a nominal rate of 40 nm/s using a relative path delay of 13.2 ns. (B) Fourier transform of the fringe pattern and the digital filter function. (C) The filtered data is shifted so the selected sideband occupies the DC location in the data array. (D) The phase of the inverse FFT of the shifted filtered data before and after unwrapping. (E) Measured laser tuning rate as a function of time.

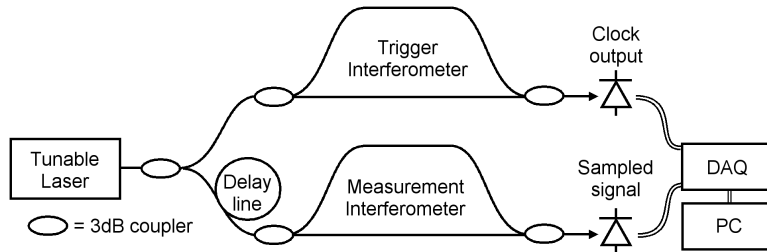


Fig. 3. Simplified schematic diagram of the SWI system used for experimental verification of sampling error correction.

and that the instantaneous value varies by nearly  $\pm 25\%$  about the mean.

#### 4. Experimental setup and results

The layout of the experimental SWI system is shown in Fig. 3. The system was built using single-mode optical fiber and components designed for use in the C telecommunications band. Not shown in the figure are polarization control and a tap that directs 2% of the laser output to an HCN wavelength reference. The bulk of the laser output is split by a 3 dB fiber coupler, sending half of the light to the measurement interferometer and half to the trigger interferometer. The trigger interferometer uses a Mach-Zehnder geometry with a group delay difference of  $\tau_t = 516$  ns between the two paths. This delay is chosen to be much less than the coherence length of the laser to avoid fringe fading due to coherence effects, but large enough such that approximation (6) is not valid. The laser wavelength is swept at a nominal rate of 40 nm/s, so for this combination of tuning rate and relative interferometer delay,  $\tau_t^2(dv/dt) \approx 1.3$ .

The measurement interferometer also uses a Mach-Zehnder geometry. The group delay difference between the two paths of this interferometer is  $\tau_m = 13.2$  ns. For this interferometer inequality (6) holds, since  $\tau_m^2(dv/dt) \approx 10^{-3}$ . Therefore the sampled fringe pattern is well described by Eq. (10) in the absence of sampling errors. Sampling errors will cause the phase of the sampled fringe pattern to deviate from linearity as a function of optical frequency.

For the first portion of this experiment, we constructed the SWI system without attention to the overall delays of the system, other than the differential delays between interferometer arms. The fringe pattern output by the measurement interferometer was sampled by the PCI-6115 DAQ card using the fringe pattern output by the trigger interferometer as an analog clock. The laser wavelength was swept from 1530 to 1538 nm at a nominal rate of 40 nm/s. To produce a plot of the phase of the sampled interferogram as a function of optical frequency we applied the following data processing steps. First, the fringe data is transformed to the time domain using the FFT algorithm. Second, a digital bandpass filter selects a 4 ns segment of the data centered on the positive delay sideband in the time domain. Third, the selected subset of the time domain data is rotated such that the peak of the sideband occupies the DC location of the 4 ns data array. Fourth, the rotated data segment is converted back to the frequency domain using an inverse FFT, resulting in complex frequency domain data. Lastly, the phase of this data is unwrapped and a linear curve fit is subtracted. The resulting measurement of the deviation from linear phase appears as the dot-dash curve in Fig. 4. The large deviation is equally present in single scan and averaged data, showing the sampling errors to be systematic in nature. The data plotted in Fig. 4 is the average of 16 measurements.

We then measured the delays associated with each optical path in the system, as well as the electronic delay between a trigger event on the analog clock photodetector and the acquisition of the corresponding datum. Optical delays were measured by incorporating the path length

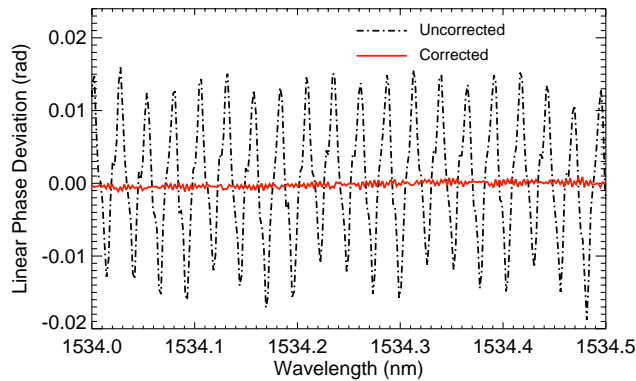


Fig. 4. (Color online) Measured linear phase deviation data for a swept-wavelength interferometer using the frequency-sampling method. The dot-dash curve shows significant error due to sampling errors for a system with unmatched system delays. These errors are present both in single-scan and averaged data. The solid red curve shows a corrected measurement of linear phase deviation using a system with an optical delay line for sampling error correction.

to be measured into a Mach-Zehnder interferometer using two 3 dB couplers. The relative delay of the interferometer was measured with and without the additional path length to be measured by counting fringes as the laser input is swept between two known wavelengths. We used an HCN wavelength reference to provide known wavelength features. This measurement technique provides accuracy of better than 1 ns even when inequality (6) does not hold because the laser tuning rate variations are oscillatory, as shown in Fig. 2(E). Tuning rate variations that oscillate about the mean rate cause the sampling errors, described by Eq. (16), to cancel out over a large number of samples. Expressed another way, while the sample spacing is not equal due to sampling errors, the average sample spacing will be  $\tau^{-1}$  because the sampling errors average to zero for the given laser tuning characteristics.

The electronic delay associated with the DAQ hardware was measured by splitting a sinusoidally modulated laser signal and sending equal parts to the trigger detector and the measurement detector. By sampling the same signal that is used for triggering, the difference between the sampled voltage and the trigger threshold voltage determines the delay between a trigger event and an acquisition event according to

$$\delta t_e = \frac{\sin^{-1} V/A}{2\pi f}, \quad (18)$$

where  $V$  is the sampled voltage level,  $A$  is the amplitude of the modulated signal, and  $f$  is the modulation frequency. The modulation frequency was chosen to correspond to the average sampling frequency that results from using the trigger interferometer with  $\tau_t = 516$  ns and a laser tuning rate of 40 nm/s.

Measurement of all system delays determined that before correction the overall  $\delta t$  for the system was  $567 \pm 5$  ns. The uncertainty associated with this value is dominated by the uncertainty in the measurement of the electronic delay. Since a value of  $\tau_t/2 = 258$  ns is necessary to correct sampling errors, and addition of delay to the measurement path contributes negative delay to  $\delta t$ ,  $309 \pm 5$  ns must be added to the measurement path.

Next we modified the SWI system to incorporate a delay line as shown in Fig. 3. We took repeated measurements of the fringe pattern at the output of the measurement interferometer for

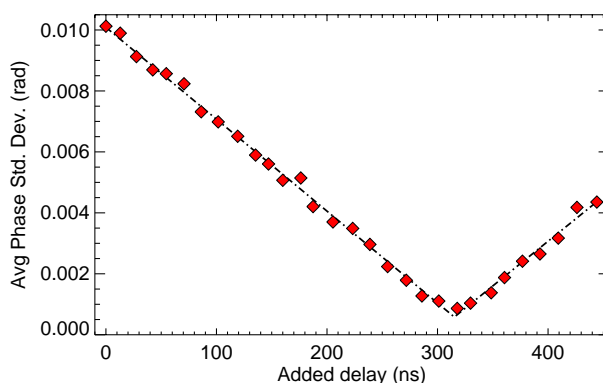


Fig. 5. (Color online) Standard deviation of the deviation from linear phase of the measured fringe pattern as a function of added delay. The filled diamonds are measured data and the dot-dash line is a piecewise linear fit.

various delay lines ranging in length from zero to 445 ns. For each measurement we recorded the standard deviation of the deviation from linear phase. The uncertainty in these data was  $\pm 0.2$  mrad, due primarily to external vibration coupling into the measurement. The results are plotted in Fig. 5. The intersection of a piecewise linear fit locates the minimum error at an added delay of  $315 \pm 14$  ns, which is in good agreement with the calculated value of  $309 \pm 5$  ns. Linear phase deviation data for the optimally corrected case is shown as the solid red curve in Fig. 4.

## 5. Summary and conclusions

We have derived analytic expressions for two sources of sampling errors that can occur when using the frequency-sampling method to trigger data acquisition in swept-wavelength measurements when the laser tuning rate is not constant. One source is intrinsic in the physics of a swept-wavelength interferometer when the path length difference and average laser tuning rate are large enough such that the approximation  $\tau^2(d\nu/dt) \ll 1$  is no longer valid. The second source can be present even for small path length differences and tuning rates and is due to transmission delays in data acquisition hardware. We further show that by introducing an optical delay line into the swept-wavelength measurement system, these errors can effectively cancel one another to second order. This eases the restrictions on the interferometer delay and laser tuning curve necessary for using the frequency-sampling method from  $\tau^2(d\nu/dt) \ll 1$  to  $\tau^3(d^2\nu/dt^2) \ll 1$ . In the case where intrinsic sampling errors are negligible, errors due to DAQ delays can be removed by using the delay line to match the measurement channel path length to the trigger channel path length. Correction of sampling errors was experimentally verified, showing an order of magnitude improvement in the phase error of the sampled interferogram.